Catalysis Letters Vol. 112, Nos. 3–4, December 2006 (© 2006)
DOI: 10.1007/s10562-006-0208-6

Influence of lanthanum carbonate phases of $Ni/La_{0.98}Sr_{0.02}O_x$ catalyst over the oxidative transformation of methane

Serbia M.A. Rodulfo-Baechler, Wilfredo Pernía, Ismael Aray, Humberto Figueroa, and Sergio L. González-Cortés*

Laboratorio de Cinética y Catálisis, Departamento de Química, Facultad de Ciencias, Universidad de Los Andes, Mérida, 5101, Venezuela

Received 18 July 2006; accepted 10 October 2006

This work combines the advantages of ~2 mol.% Sr/La_2O_3 (i.e. $La_{0.98}Sr_{0.02}O_x$) for OCM (oxidative coupling of methane) with well-dispersed nickel over metal oxides for POM (partial oxidation of methane) to efficiently transform methane to desirable products. The catalysts were prepared by sequential impregnation and characterized by X-ray diffraction, thermogravimetric analysis, scanning electron microscopy, temperature-programmed reduction, temperature-programmed decomposition of carbonates and BET surface area measurements. The aim of this work is to find out not only the effect of the catalyst compositions over the formation and growth of carbonate phases, but also their influence over the transformation oxidative of methane.The $La_{0.98}Sr_{0.02}O_x$ – supported Ni catalyst precursors show a strong nickel oxide–lanthana interaction, involving anionic vacancies or structural defects that induce the formation of island-like structure of $La_{2-x}Sr_xNiO_4$-type mixed oxide for 2 mol.% $Ni/La_{0.98}Sr_{0.02}O_x$. Higher nickel composition facilitates the formation of $LaNiO_3$. Surface lanthanum hydroxycarbonate formation is probably associated with a conjugated effect between lanthanum oxide and oxidized nickel phases. For high-nickel amount containing catalysts, carbonate-enriched $La_2(OH)_{6-2x}(CO_3)_x$ as intermediate phase in methane reforming reaction is proposed. For low nickel composition (i.e. 2%), partial oxidation of methane could follow predominantly the pyrolysis mechanism. In which, carbon monoxide is the direct product and carbon dioxide is subsequently formed from carbon monoxide oxidation.

KEY WORDS: methane; Ni-containing catalysts; oxidative transformation of methane; lanthana.

1. Introduction

The direct conversion of methane to ethane and ethylene (C_2) for oxidative coupling of methane (OCM) on Sr-promoted La_2O_3 catalyst has been widely studied [1–3]. This catalyst has shown a high C_2 selectivity, owing to its high basicity. Also, the modification of lanthanum oxide with Sr^{2+} ion, whose ionic radius (R_{Sr} = 1.12 Å) is similar to that of La^{3+} (R_{La} = 1.14 Å), produces an increase in oxygen lattice mobility due to the formation of anionic vacancies [4]. Le Van *et al*. [2] proposed that the main role of strontium to high calcination temperature (800–950 °C) could be textural, retarding the sintering and preserving the platelet shape of oxide particles and high C_2 selectivity. Even thought this catalyst has shown acceptable yields of C_2 products, additional research is needed to integrate advanced separation technology with novel reactor designs. Furthermore, the empirical evidences for oxidative coupling of methane suggest that the maximum yield is about 30% in a conventional reactor. This is attributed to the effect of gas-phase reactions or the lack of selective low-temperature catalysts that could operate under conditions in which gas-phase reactions are not significant [5].

In view that the uselfuness of direct conversion of methane has been limited, the carbon dioxide reforming of methane (CDRM) and the partial oxidation of methane (POM) to synthesis gas (CO/H_2) have attracted significant attention during the last years [6,7] Since syngas is a versatile feedstock in many industrial synthetic processes and easily transformed to either methanol [8] or hydrocarbons via the Fischer–Tröpsch reaction [9]. These catalytic routes could let to transform the large worldwide natural gas reserves, whose principal component is methane, into more valuable chemicals and fuels.

Nickel-based catalysts have been studied in the partial oxidation of methane (POM) to syngas [10,11]. Tsipouriari et al. [12,13] found that a Ni/La_2O_3 catalyst exhibited good activity and excellent stability compared with conventional nickel catalysts. They also determined that carbon species were deposited in the form of Ni_3–C, Ni–CO_3, and $La_2O_2CO_3$. On the other hand, the dry reforming of methane is an attractive catalytic process for environmental protection because both reactants are greenhouse gases. The noble metal catalysts have shown to be efficient for this catalytic reaction. However, catalyst development with lower cost metals (Fe, Co, and Ni) seems to be more desirable taking into account availability and economic

*To whom correspondence should be addressed.
E-mail: goncor@ula.ve

considerations [14,15]. Since this catalytic process is highly endothermic, operating temperatures higher than 973 K are required to obtain high conversion and syngas selectivity. At these temperatures, for instance, Ni-based catalysts are susceptible to deactivation by metallic particle sintering and carbon deposition [16]. Although, Zhang and Verykios [17] showed that nickel supported on La_2O_3 and properly activated exhibited good activity and excellent stability. It was proposed that nickel and lanthanum interaction creates synergetic sites at the Ni–La_2O_3 interface, which resisted catalyst deactivation [18].

The aim of this work is to combine the advantages of ~2 mol.% Sr/La_2O_3 (i.e. $La_{0.98}Sr_{0.02}O_x$) with well-dispersed nickel over metal oxides to efficiently transform methane to desirable products. A catalyst-activation process that generates nickel upon the catalytic reaction and avoids the catalyst deactivation is applied. Emphasis on the effect of the catalyst compositions over the formation and growth of carbonate phases and mixed-metal oxides and their influence over the transformation oxidative of methane is given.

2. Experimental

2.1. Catalyst preparation

Lanthanum oxide, La_2O_3 (Sigma, 99.9%), previously calcined at 700 °C, was impregnated with strontium nitrate (Merck, 99.9%) at ca. 2 mol.% Sr ($La_{0.98}Sr_{0.02}O_x$). Then, this solid was treated with appropriate amounts of nickel nitrate (J.T. Baker, 99.9%) aqueous solutions to obtain catalysts with 2, 10 and 55 mol.% Ni (compositions verified by energy dispersive X-rays spectroscopy with a 10% maximum error). After each impregnation step, the solids were dried at 140 °C for 14 h and then calcined at 750 °C in dry, CO_2-free air stream, for 4 h. Additionally, two catalyst series with variable support compositions (SrO–La_2O_3) and calcination temperatures (i.e. 600 and 750 °C) were prepared under the above-mentioned catalyst preparation conditions.

2.2. Catalytic performance

The catalytic reactions were conducted in a packed-bed tubular quartz reactor (48 cm long, 5 mm i.d.) with an axial thermowell containing a chromel–alumel thermocouple centered in the catalyst bed. The sample (100 mg, 28–65 mesh) was activated *in situ* at 750 °C, for 1 h with a 25 mL min^{-1} dry air flow. The catalytic tests were carried out at atmospheric pressure, 700 °C, 3.6 (CH_4/O_2) molar relation feed and 1000 mL(g $min)^{-1}$ specific velocity. Gaseous products (C_1, C_2, CO_2, CO and O_2) separation and identification were done with two on-line gas chromatographs: the first with a TC detector and Carbosieve S column (30–60 mesh, 2 m long, 1/8'' external diameter) to separate oxygen, methane, carbon monoxide and carbon dioxide, the second with FID detector and silica gel column (80–100 mesh, 5 m long, 1/8'' external diameter) to separate methane and C_2 products.

2.3. Catalyst characterization

The crystalline phases of the catalysts were identified by X-ray diffraction (XRD) in a Siemens D5005 diffractometer with θ:θ geometry, using CuKα radiation (λ = 1.54059 Å) and conditions of 40 kV and 30 mA. The specimens were prepared by grinding a small amount of each sample using agate mortar and pestle and then loaded into a flat sample holder.

Semi-quantitative analysis of the catalyst series was carried out by energy-dispersive X-rays spectroscopy (EDXS) using a Kevex model Delta-3 system connected to a Hitachi model S-2500 scanning electron microscope. This instrument was also employed to find out the influence of the support composition over the catalyst morphology.

In order to determine the stoichiometric composition of the lanthanum hydroxycarbonate, after the catalytic reaction the $La_{0.98}Sr_{0.02}O_x$-supported Ni catalysts were studied by thermogravimetric (TG) from room temperature to 850 °C, using a 175 mL min^{-1} air flow and 20 °C min^{-1} heating rate.

BET specific surface areas were measured in a Quantasorb Jr., QS JR-2 Model, by the multiple point method. The sample was degassed at 350 °C for 4 h, before exposing the solid to the N_2–He mixture. The BET area for $La_{0.98}Sr_{0.02}O_x$ was 11 m^2/g, whereas for 2% Ni-, 10% Ni- and 55% Ni-containing catalysts were 12, 15 and 7 m^2/g, respectively.

Temperature programmed reduction (TPR) was carried out on a Micromeritics TPD/TPR 2900 system; the samples were pre-treated before analysis with a dry air flow rate of 30 mL min^{-1} for 1 h at 750 °C to eliminate adsorbed water and carbon dioxide. The TPR runs were done with a reducing H_2–Ar mixture (10% H_2), 25 mL min^{-1} flow rate and 5 °C min^{-1} heating rate. A sample weight was selected to work within the Malet and Caballero conditions [19].

Thermal decomposition of carbonates (TDC) was also conducted on a Micromeritics TPD/TPR 2900 system. The samples (ca. 100 mg) were pretreated to 750 °C for 1 h under either flowing air (oxidized state) or flowing hydrogen (reduced state). The catalysts were cooled down to 25 °C and then treating with carbon dioxide to 500 °C for 30 min. The TDC runs were carried out using a helium flow rate of 50 mL/min and heating rate of 10 °C.min^{-1} from room temperature up to 850 °C.

3. Results and discussion

In Table 1 is summarized the methane conversion, products distribution and the different phases of the

Table 1
Catalytic performance, hydroxycarbonate phases and crystalline phases of $Ni/La_{0.98}Sr_{0.02}O_x$ catalysts

Ni loading (mol.%)	[a]XCH_4 (mol.%)	SC_2 (mol.%)	SCO (mol.%)	SCO_2 (mol.%)	XRD phase	[b]Hydroxycarbonate phase
0	23.2	51.7	14.3	34.0	$La(OH)_3$*, La_2O_3	$La_2(OH)_{4.4}(CO_3)_{0.8}$
2	19.0	12.4	50.2	37.4	$La(OH)_3$*, La_2O_3	$La_2(OH)_{3.8}(CO_3)_{1.1}$
10	36.4	1.5	76.4	22.1	$La(OH)_3$*, $LaNiO_3$	$La_2(OH)_{2.6}(CO_3)_{1.7}$
55	38.1	0.1	85.3	14.6	$LaNiO_3$*, NiO	$La_2(OH)_{2.2}(CO_3)_{1.9}$

[a]Catalytic reactions conducted at 700 °C and CH_4 to O_2 ratio of 3.6. [b]Stoichiometric ratio determined by TG analysis after the catalytic tests. *Major crystalline phase.

$La_{0.98}Sr_{0.02}O_x$-supported Ni catalysts. The Ni-containing solids showed early activation in the catalytic reaction (ca. 1–2 h) and no sign of deactivation during the time on stream (10 h). It is clearly illustrated that the Ni loadings strongly affect the catalytic behavior of $La_{0.98}Sr_{0.02}O_x$ catalyst. The addition of 2 mol.% Ni produces a slight decrease in CH_4 conversion with a notable increase in CO selectivity. This is likely due to the partial oxidation of C_2, since the CO_2 selectivity does not change significantly compared with $La_{0.98}Sr_{0.02}O_x$. Nickel loadings above 2 mol.% not only improve the methane conversion, but also the selectivity to CO as the CO_2 selectivity and particularly to C_2 were strongly diminished. As we expected, further nickel to $La_{0.98}Sr_{0.02}O_x$ generates an additional catalytic pathway that facilitates the conversion of methane to synthesis gas [6]. This is due to the formation of Ni particles during the time on stream. The calcined $La_{0.98}Sr_{0.02}O_x$ and Ni-containing catalysts (up to 10 mol.%) present lanthanum hydroxide as major crystalline phase, in line with the high tendency of lanthana to absorb carbon dioxide and water [20]. A minor mixed oxide phase was also observed in 10 mol.% Ni-containing catalyst. In contrast, the 55% Ni-loading catalyst shows $LaNiO_3$ perovskite phase with rhombohedral structure as the most prominent crystalline structure [21] and NiO as minor phase. No strontium phases were detected owing to either the incorporation of Sr^{2+} into the La_2O_3 structure or its low content on the lanthanum oxide.

It is well-established that lanthana present a high ability to absorb CO_2 and H_2O. The characterization of used La_2O_3-based catalysts by TG analysis can therefore provide important details about the role played by those molecules during the oxidative transformation of methane. According to previous reports [20,22], lanthana stabilized in air would consist of poorly crystallized It is therefore reasonable to expect the formation of hydroxycarbonate phases during the catalytic reaction, owing to the methane–oxygen interaction on the lanthana surface. Table 1 also shows the influence of the Ni loadings over the stoichiometric composition of the hydroxycarbonate phases. This ratio was determined using the weight losses associated with desorption of water and carbon dioxide upon the thermal treatment [20,23]. It is worth remarking that the hydroxycarbonate phase compositions for $La_{0.98}Sr_{0.02}O_x$ and 2 mol.% $Ni/La_{0.98}Sr_{0.02}O_x$ catalysts trend to the formation of $La_2(OH)_4(CO_3)$. For 10 mol.% $Ni/La_{0.98}Sr_{0.02}O_x$ and 55 mol.% $Ni/La_{0.98}Sr_{0.02}O_x$ a stoichiometry close to $La(OH)(CO_3)$ was obtained. Scheme 1 illustrates this tendency.

$$La_2(OH)_4(CO_3) \xleftarrow{x\sim 1} La_2(OH)_{6-2x}(CO_3)_x \xrightarrow{x\sim 2} 2La(OH)(CO_3) \quad (1)$$

Indeed, results obtained by FT-IR spectroscopy (no shown) revealed a clear increase of the carbonate phase and reduction of the hydrate phase as rising nickel loading, supporting the scheme (1). These findings allow one to suggest that the presence of hydroxycarbonate phases might play an important role in the oxidative transformation of methane on lanthana-based catalysts.

Temperature-programmed reduction profiles of the $La_{0.98}Sr_{0.02}O_x$–supported nickel catalysts are shown in figure 1. In order to compare the different reduction stages, the TPR profiles of the bulky NiO and $LaNiO_3$ are included. Nickel oxide shows a hydrogen consumption peak near 360 °C, corresponding to a Ni^{2+} to nickel reductive process (Figure 1a). The TPR profile of $LaNiO_3$ mixed oxide shows two reduction steps at 330 and 455 °C with an area ratio of 2 (Figure 1b). The lower temperature peak is associated with the formation of $La_2Ni_2O_5$ (or $LaNiO_{2.5}$) through the reduction of Ni^{3+} to Ni^{2+}. The second peak at higher temperature corresponds to the reduction of Ni^{2+} to metallic nickel [24,25]. The 2% nickel catalyst reduction profile shows four peaks: The α and β_1 peaks (300 and 335 °C, respectively) are attributed to amorphous NiO and the first reduction step of mixed oxide phase, respectively. A small β_2 peak at intermediate temperature (β_2) (maximum at 425 °C) is tentatively assigned to reduction of NiO crystallites interacting with strontium oxide. An asymmetric major broad reduction peak (γ) at higher temperature ($\sim$ 565 °C), can be associated with reduction of a new phase formed by NiO solid-state reaction with La_2O_3. This process might occur over anionic vacancies created by La^{3+} substitution for Sr^{2+} in the solid [4,26], leading to the formation of island-like structure of $LaSrNiO_x$ mixed oxide. For 10% nickel catalyst, β_1-peak intensity slightly increases and the β_2 peak disappears, owing to the relatively low Sr^{2+} composition compared with increasing Ni

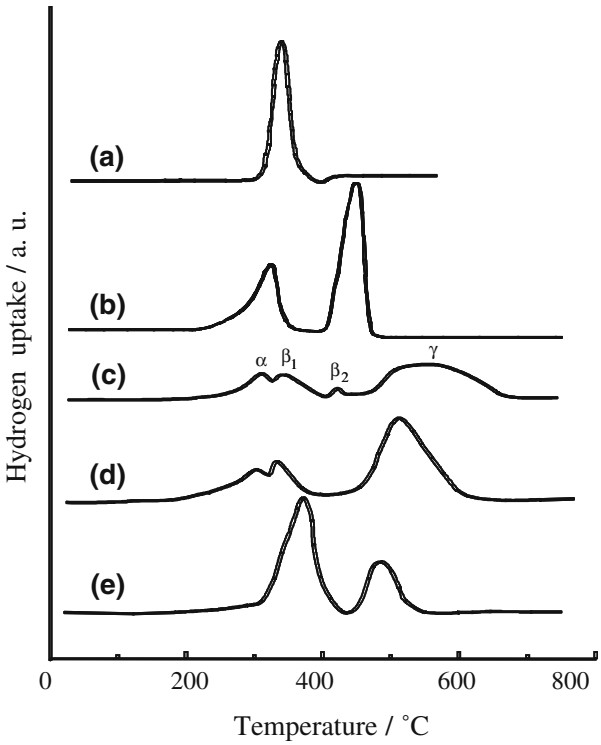

Figure 1. Effect of nickel loadings on the TPR profiles of Ni/$La_{0.98}Sr_{0.02}O_x$ catalyst precursors. (a) NiO, (b) $LaNiO_3$, (c) 2% Ni, (d) 10% Ni, (e) 55% Ni.

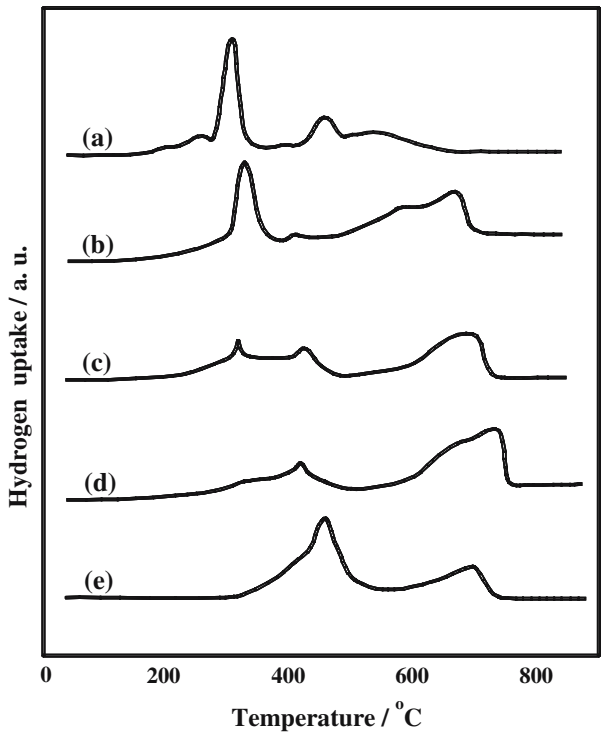

Figure 2. Effect of strontium loadings on the TPR profiles of 17 mol.% NiO/SrO–La_2O_3 calcined at 600 °C. (a) NiO/La_2O_3, (b) 6% Sr, (c) 27% Sr, (d) 43% Sr , (e) 83% Sr.

loading. Furthermore, the γ peak becomes more symmetric and a slight decrease in reduction temperature is observed (Figure 1d). This profile confirms the presence both of $LaNiO_3$ phase and poorly-crystallized NiO. The TPR profile of 55% nickel catalyst shows a lower temperature peak that corresponds to NiO reduction and reductive process of Ni^{3+} going to Ni^{2+}. The higher temperature peak to Ni^{2+} reduction to metallic Ni is also observed (Figure 1e).

In order to find out the influence of Sr^{2+} ions over the mixed oxide formation, a catalyst series of 17 mol.% Ni supported on different SrO–La_2O_3 proportions was prepared and characterized by temperature-programmed reduction, figure 2. The addition of Sr^{2+} ions to NiO/La_2O_3 catalyst produces a clear descent of the species reduced at low reduction temperature, characteristics of free NiO. A concomitant increase not only of the peak intensity, but also the temperature of the high-temperature reduction peak is also observed. This is attributed to the formation of $La_{2-x}Sr_xNiO_4$ perovskite-type mixed oxide [27], as was confirmed by powder X-ray diffraction. Furthermore, an intermediate-temperature reduction peak at ca. 420 °C is defined with increasing Sr^{2+} loading and reaches a maximum intensity in the catalyst without lanthana. This tendency supports the proposal that a SrO–NiO interaction takes place, owing to either counter-diffusion of Sr^{2+} and Ni^{2+} ions or to dissolution-precipitation process in the vicinity of the strontium oxide surface.

The effect of the support compositions over the BET specific surface area (S_{BET}) is shown in figure 3. Addition of small amount of SrO (i.e. 6 mol.%) to NiO/La_2O_3 catalyst produces a slight increase of the S_{BET}, however further SrO content markedly decreases the surface area up to 3 $m^2\ g^{-1}$. These textural changes are reflected in the catalyst morphology and particle size (Figure 4). Indeed, the SEM image of 17 mol.% NiO/La_2O_3 (Figure 4a) shows a major platelet shape mor-

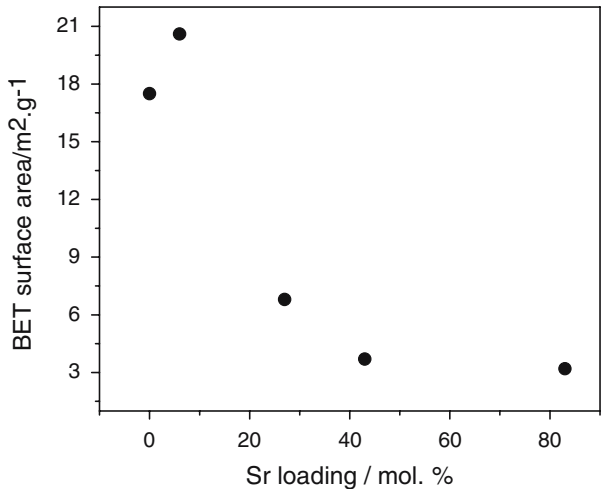

Figure 3. Variation of the BET specific surface areas of 17 mol.% NiO/SrO–La_2O_3 with support composition.

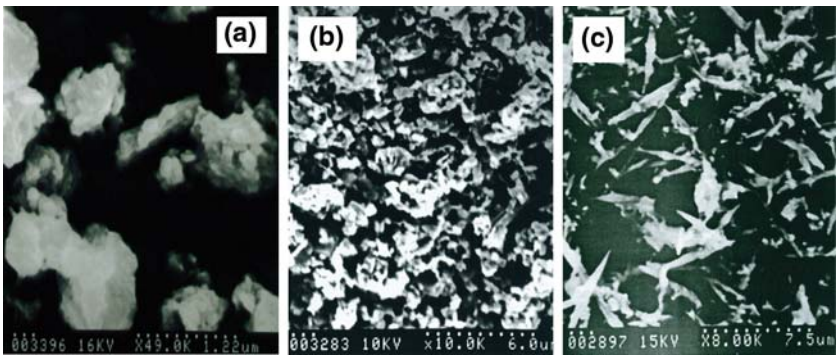

Figure 4. SEM images of 17 mol.% NiO/SrO–La_2O_3 catalysts. (a) 0% Sr, (b) 27% Sr, (c) 83% Sr.

phology, owing to the high content of lanthana [2], whereas the ternary Ni–Sr–La–O system (27 mol.% Sr) shows compact aggregation of particles with average particle size clearly greater than NiO/La_2O_3 catalyst (Figure 4b). On the other hand, the binary Ni–Sr–O catalyst illustrates an needle-type morphology, which is clearly different that the above catalysts. Therefore, the catalyst composition not only affects the interaction among the catalyst components and the textural characteristics, but also the catalyst morphology as result of different particle aggregation degrees.

A catalyst series with 10 mol.% Ni and variable support composition was calcined a 750 °C and analyzed by temperature-programmed reduction, figure 5. It is clearly illustrated that the addition of strontium increases the reduction temperature of the high-temperature peak compared with the Sr^{2+}-free catalyst. Particularly at high Sr content because of the formation of $La_{2-x}Sr_xNiO_4$ mixed oxide. This finding is in line with the idea that the addition of Sr^{2+} even at very low loading (ca. 2 mol.%) facilitates the mixed metal oxide formation. This is associated with the presence of anionic vacancies created by La^{3+} substitution for Sr^{2+} in the lanthana [4,26], leading to the formation of island-like structure of $La_{2-x}Sr_xNiO_4$-type mixed oxide. This tendency also indicates that the $LaNiO_3$ phase, presents in the sample without Sr, shows a higher reducibility than $La_{2-x}Sr_xNiO_4$ mixed oxide.

The TPR profiles of the Ni-containing catalysts after the oxidative transformation of methane are displayed in figure 6. The reduction profile for the 2% nickel catalyst, (figure 6a), shows an enrichment of bulky NiO (centered at 356 °C) and a decrease of the less reducible nickel phase (600 °C) compared with the catalyst before reaction, figure 1c. This is attributed to the partial reduction of the mixed oxide during the time on stream, facilitating the NiO segregation. With increasing Ni loading, the low-reduction temperature peak becomes higher whereas the peak at higher reduction temperature (γ peak) starts to be broader. This tendency suggests that the increase of the nickel loading favors the formation of different nickel oxidized species during catalytic reaction, particularly NiO. This facilitates total methane combustion [28]. The total hydrogen uptake ratio before to after the catalytic reaction shows the following order: 2.6 (2% Ni) < 0.9 (10% Ni) < 0.7 (55% Ni). The higher ratio (i.e. 2.6) can be rationalized assuming hydrogen consumption by reactive surface carbon generated during the catalytic tests [13,29]. The hydrogen uptake ratio below one, on the other hand, can be attributed to the formation both of partially and totally reduced nickel-containing phases, which are produced by the oxygen concentration decreases along the catalyst bed [28,30].

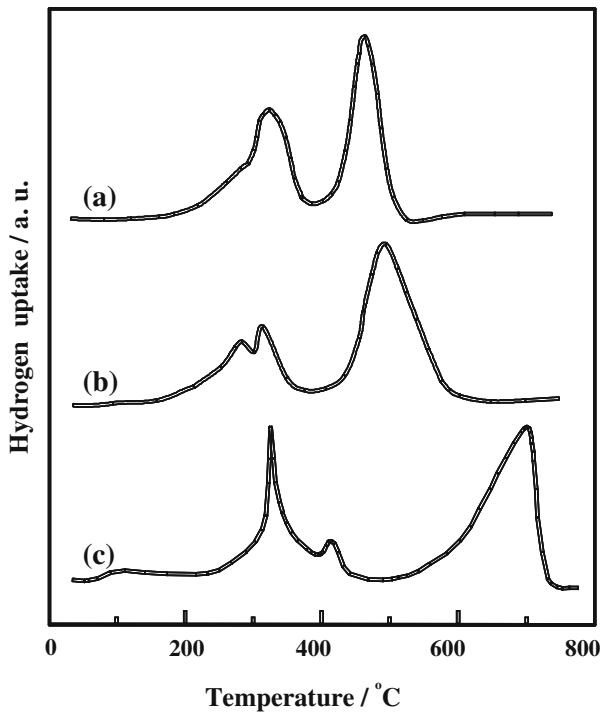

Figure 5. Effect of strontium loadings on the TPR profiles of 10 mole% NiO/SrO–La_2O_3 calcined at 750 °C. (a) 10% Ni/ La_2O_3, (b) ~2% Sr, (c) 21% Sr.

The thermal decomposition profiles of the carbonate phases for $Ni/La_{0.98}Sr_{0.02}O_x$ catalyst are illustrated in figure 7. For Ni-containing catalysts up to 10%, a major

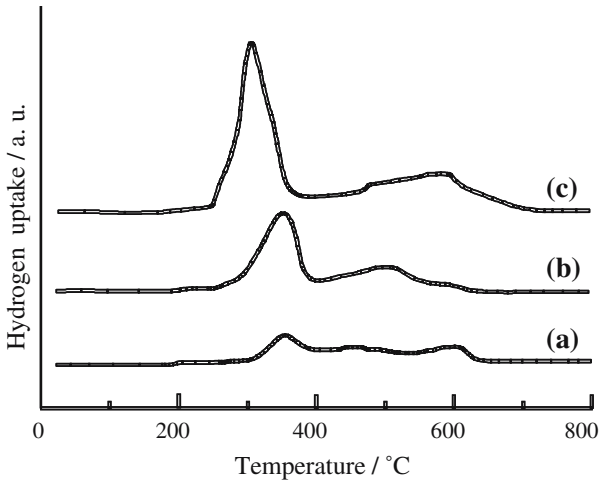

Figure 6. TPR profiles of the $La_{0.98}Sr_{0.02}O_x$-supported nickel catalysts after catalytic tests. (a) 2% Ni, (b) 10% Ni, (c) 55% Ni.

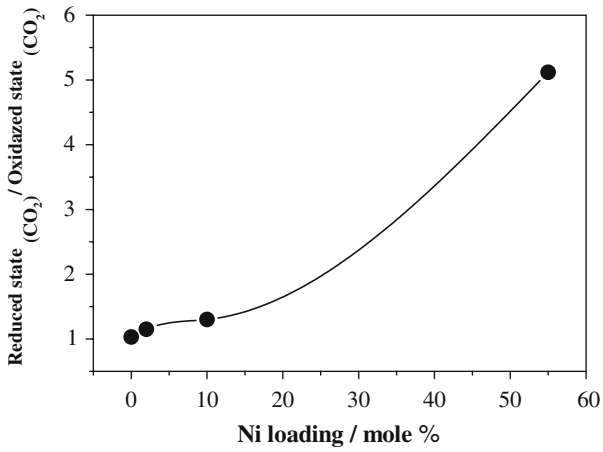

Figure 8. Dependence of the CO_2 ratio from the reduced to oxidized sample with different Ni loadings.

peak centered at approximately 770–760 °C is observed. This feature is assigned to the thermal decomposition of lanthanum dioxomonocarbonate ($La_2O_2CO_3$). The profile of 55% Ni catalyst displays a very small peak, whose temperature was markedly reduced compared with the above-mentioned catalysts. The reduced catalyst series, on the other hand, presented a similar behavior than that of oxidized catalysts, particularly for low Ni compositions. Since at high Ni loading (i.e. 55%) a strong difference not only on the peak position, but also on the content of carbonate phase was observed, see inset in figure 7. Indeed, the total amount of CO_2 generated by $La_{0.98}Sr_{0.02}O_x$ and 2% $Ni/La_{0.98}Sr_{0.02}O_x$ catalysts during the decomposition process coincides rather well with the stoichiometric composition of

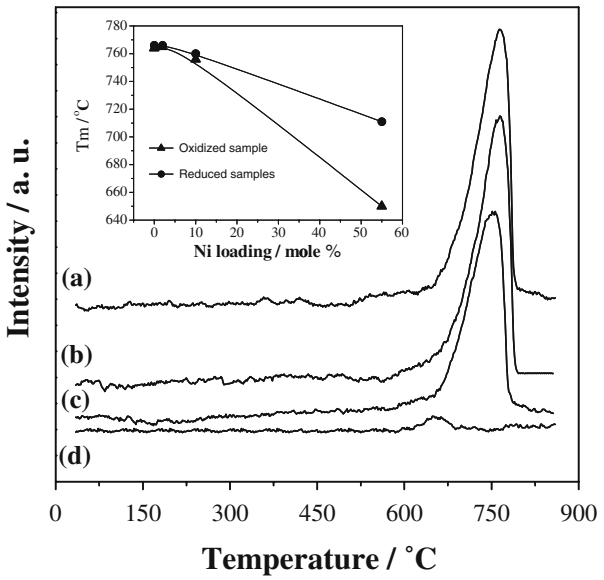

Figure 7. Thermal decomposition profiles of carbonate phases of the $La_{0.98}Sr_{0.02}O_x$-supported nickel catalysts. (a) 0% Ni, (b) 2% Ni, (c) 10% Ni, (d) 55% Ni.

$La_2O_2CO_3$. However, the 10% Ni- and 55% Ni-containing catalysts present a lower content of CO_2 than that generated by the thermal decomposition of dioxomonocarbonate phase, particularly 55% Ni catalyst. This finding is in line with the poor CO_2 adsorption capability of La–Ni mixed oxide compared with lantana [31]. The influence of the Ni loadings over the CO_2 ratio produced by the reduced and oxidized samples is illustrated in figure 8. The amount of CO_2 produced upon the thermal decomposition process is strongly improved for reduced 55% Ni catalyst compared with the oxidic-state sample, as Ni-containing catalysts with compositions below 55% showed CO ratios rather similar and close to one (i.e. 1.0–1.3). This finding together with the TGA and TPR results suggests that the formation of carbonate-enriched hydroxycarbonate phases during the oxidative transformation of methane is consequence of the partial reduction process underwent by the catalyst upon catalytic reaction.

The reaction between methoxide ions, formed from the reaction of methyl radicals with lanthanum oxide structural defects [32], and oxygen centres continued by a series of surface oxidation steps can lead to the lanthanum hydroxycarbonate formation. The partially oxidized nickel phases facilitate the formation of carbonate-enriched $La_2(OH)_{6-2x}(CO_3)_x$, probably due to the presence of lanthanum oxide highly enriched with structural defects. Indeed, the catalytic tests show that nickel loading improves syngas formation instead of carbon dioxide (see table 1). This fact strongly suggests that lanthanum hydroxycarbonate is an intermediate phase in methane reforming reaction, especially for high-nickel containing catalysts, probably through hydroxycarbonate phase decomposition with C–Ni entities [29]:

$$C-Ni_n + La(OH)CO_3 \rightarrow 2CO + Ni_n + \frac{1}{2}La_2O_3 + \frac{1}{2}H_2O \quad (2)$$

For the lower nickel composition (2%), partial oxidation of methane could follow predominantly the pyrolysis mechanism. Carbon monoxide is the direct product and carbon dioxide is subsequently formed from carbon monoxide oxidation [33]. The decomposition reaction of hydroxycarbonate phases has been used to explain carbon dioxide formation in methane transformation on lanthanum oxide [32], whereas dioxymonocarbonate decomposition with active surface carbon was suggested as a carbon monoxide generating source [18]. In this work, we put forward further evidences about the hydroxicarbonate role in the oxidative transformation of methane on $La_{0.98}Sr_{0.02}O_x$-supported Ni catalysts.

4. Conclusions

The addition of approximately 2 mol.% of Sr^{2+} ions over lanthanum oxide facilitates the La_2O_3–NiO interaction, owing to the presence of anionic vacancies created by La^{3+} substitution for Sr^{2+} in the lanthana. This solid state reaction leads to the formation of island-like structure of $La_{2-x}Sr_xNiO_4$-type mixed oxide for 2 mol.% $Ni/La_{0.98}Sr_{0.02}O_x$. Furthermore, Sr^{2+}–NiO interaction might favor a decorative effect of the NiO particles by Sr^{2+} species. The catalyst formulation not only affects the interaction among the catalyst components and the textural characteristics, but also the catalyst morphology. The formation of bimetallic or trimetallic mixed metal oxides strongly alter the reducibility of $La_{0.98}Sr_{0.02}O_x$-supported Ni catalyst precursors compared with lanthana-supported nickel oxide.

At high nickel loadings, the formation of surface lanthanum hydroxycarbonate enriched with carbonate (i.e., $La(OH)CO_3$) is enhanced. This is probably associated with the formation of lanthanum oxide and partially oxidized nickel phases during the catalytic reaction. The hydroxycarbonate phase formation from methane oxidation over anionic vacancies and coordinatively unsaturated oxygen atoms is proposed. Carbonate-enriched $La_2(OH)_{6-2x}(CO_3)_x$ seems to be an intermediate phase in methane reforming reaction. For low nickel composition (2%), however, partial oxidation of methane could follow predominantly the pyrolysis mechanism. Car bon monoxide is the direct product and carbon dioxide is subsequently formed from carbon monoxide oxidation.

Acknowledgments

This work was financially supported by CDCHT-ULA and FONACIT. W.P., I.A. and H.F. thank to CDCHT-ULA for funding.

References

[1] J.M. DeBoy and R.F. Hicks, J. Chem. Soc., Chem. Commun. (1988) 982.
[2] T. LeVan, M. Che and J.M. Tatibouet, Catal. Lett. 14 (1992) 321.
[3] V.S. Choudhary, S.A.R. Mulla and V.H. Rane, J. Chem. Technol. & Biotechnol. 72 (1998) 125.
[4] H. Borchert and M. Baerns, J. Catal. 168 (1997) 315.
[5] V.R. Choudhary and B.S. Uphade, Catal. Surveys Asia 8 (2004) 15.
[6] Y.-H. Hu and E. Ruckenstein, Adv. Catal. 48 (2004) 297.
[7] A.P.E. York, T. Xiao and M.L.H. Green, Topics Catal. 22 (2003) 345.
[8] A. Gotti and R. Prins, J. Catal. 178 (1998) 511.
[9] S.L. González-Cortés, S.M.A. Rodulfo-Baechler, A. Oliveros, J. Orozco, B. Fontal, A.J. Mora and G. Delgado, React. Kinet. Catal. Lett., 75 (2002) 3.
[10] S.L. González-Cortés, J. Orozco, D. Moronta, B. Fontal and F.E. Imbert, React. Kinet. Catal. Lett. 69 (2000) 145.
[11] T. Hayakawa, H. Harihara, A.G. Andersen, A.P.E. York, K. Suzuki, H. Yasuda and K. Takehira, Angew. Chem. Int. Ed. Engl. 35 (1996) 192.
[12] V.A. Tsipouriari, Z. Zhang and X. Verykios, J. Catal. 179 (1998) 283.
[13] V.A. Tsipouriari and X. Verykios, J. Catal. 179 (1998) 292.
[14] S.C. Tsang, J.B. Claridge and M.L.H. Green, Catal. Today 23 (1995) 3.
[15] X.-W. Chen, T.-C. Xiao, S.L. González-Cortés and M.L.H. Green, Chem. Res. Chinese U. 20 (2004) 457.
[16] S. Wang, G.Q. Li and G.J. Millar, Energy & Fuels 10 (1996) 896.
[17] Z. Zhang and X. Verykios, J. Chem. Soc., Chem. Commun. (1995) 71.
[18] Z. Zhang, X. Verykios, S.M. MacDonald and S. Affrossman, J. Phys. Chem. 100 (1996) 744.
[19] P. Malet and A. Caballero, J. Chem. Soc. Faraday Trans. 84 (1988) 2369.
[20] S. Bernal, J.A. Diaz, R. García and J.M. Rodríguez-Izquierdo, J. Mater. Sci. 20 (1985) 537.
[21] H. Obayashi and T. Kudo, Japan J. Appl. Phys. 14 (1975) 330.
[22] S. Bernal, G. Blanco, J.J. Calvino, J.A. Pérez Omil and J.M. Pintado, J. Alloys Compd. 408–412 (2006) 496.
[23] S. Bernal, F.J. Botana, R. Garcia, F. Ramírez and J.M. Rodríguez-Izquierdo, J. Mater. Sci. 22 (1987) 3793.
[24] M. Crespin, P. Levitz and L. Gatineau, J. Chem. Soc. Faraday Trans. 79 (1983) 1181.
[25] J. Requies, M.A. Cabrero, V.L. Barrio, M.B. Güemez, J.F. Cambra, P.L. Arias, F.J. Pérez-Alonso, M. Ojeda, M.A. Pena and J.L.G. Fierro, Appl. Catal. A Gen. 289 (2005) 214.
[26] M.S. Islam and D.J. Ilett, J. Phys. Chem. 98 (1994) 9637.
[27] J. Rynkowski, P. Samulkiewic, A.K. Ladavos and P.J. Pomonis, Appl. Catal. A Gen. 263 (2004) 1.
[28] D. Dissanayake, M.P. Rosynek, K.C.C. Kharas and J.H. Lunsford, J. Catal. 132 (1991) 117.
[29] S.L. González-Cortés, J. Orozco and B. Fontal, Appl. Catal. A Gen. 213 (2001) 259.
[30] F. van Looij and J.W. Geus, J. Catal. 168 (1997) 154.
[31] S.L. González-Cortés, B. Fontal and D. Moronta, Rev. Mex. Fís. 47 (2001) 367.
[32] S. Lacombre, C. Geantet and C. Mirodatos, J. Catal. 151 (1994) 439.
[33] Y.H. Hu and E. Ruckenstein, J. Catal. 158 (1996) 260.